IOPscience iopscience.iop.org

Home Search Collections Journals About Contact us My IOPscience

Dimer site-bond percolation on a triangular lattice

This content has been downloaded from IOPscience. Please scroll down to see the full text.

View the table of contents for this issue, or go to the journal homepage for more

Download details:

IP Address: 200.130.19.183
This content was downloaded on 11/02/2017 at 12:11

Please note that terms and conditions apply.

You may also be interested in:

Site-bond percolation on simple cubic lattices: numerical simulation and analytical approach
M I González, P M Centres, W Lebrecht et al.

Inverse percolation by removing straight rigid rods from square lattices
L S Ramirez, P M Centres and A J Ramirez-Pastor

Percolation and jamming in random sequential adsorption of linear k-mers on square lattices with the presence of impurities
P M Centres and A J Ramirez-Pastor

Site-bond percolation: a low-density series study of the uncorrelated limit
P Agrawal, S Redner, P J Reynolds et al.

Thermal percolation for interacting monomers adsorbed on square lattices
M C Giménez, F Nieto and A J Ramirez-Pastor

Critical behaviour of AB percolation in two dimensions
H Nakanishi

Site percolation on lattices with low average coordination numbers
Ted Y Yoo, Jonathan Tran, Shane P Stahlheber et al.

A new scale-invariant ratio and finite-size scaling for the stochastic susceptible–infected–recoveredmodel
David R de Souza, Tânia Tomé and Robert M Ziff

Correlated percolation and the correlated resistor network
Paul J M Bastiaansen and Hubert J F Knops

Journal of Statistical Mechanics: Theory and Experiment
An IOP and SISSA journal

PAPER: Classical statistical mechanics, equilibrium and non-equilibrium

Dimer site-bond percolation on a triangular lattice

L S Ramirez[1], N De la Cruz Félix[1,2], P M Centres[1] and A J Ramirez-Pastor[1]

[1] Departamento de Física, Instituto de Física Aplicada, Universidad Nacional de San Luis-CONICET, Ejército de Los Andes 950, D5700HHW, San Luis, Argentina

[2] Departamento de Física, Instituto de Física (IFIS), Universidad Autónoma de Santo Domingo (UASD), Av Alma Mater, Santo Domingo 81000, Republica Dominicana

E-mail: antorami@unsl.edu.ar

Received 18 November 2016, revised 31 December 2016
Accepted for publication 10 January 2017
Published 6 February 2017

Online at stacks.iop.org/JSTAT/2017/023206
doi:10.1088/1742-5468/aa58f2

Abstract. A generalization of the site-percolation problem, in which pairs of neighbor sites (site dimers) and bonds are independently and randomly occupied on a triangular lattice, has been studied by means of numerical simulations. Motivated by considerations of cluster connectivity, two distinct schemes (denoted as $S \cap B$ and $S \cup B$) have been considered. In $S \cap B$ ($S \cup B$), two points are said to be connected if a sequence of occupied sites *and* (*or*) bonds joins them. Numerical data, supplemented by analysis using finite-size scaling theory, were used to determine (*i*) the complete phase diagram of the system (phase boundary between the percolating and nonpercolating regions), and (*ii*) the values of the critical exponents (and universality) characterizing the phase transition occurring in the system.

Keywords: numerical simulations, percolation problems

© 2017 IOP Publishing Ltd and SISSA Medialab srl

J. Stat. Mech. (2017) 023206

Contents

1. Introduction **2**

2. The model **4**

3. Simulation scheme **5**

4. Percolation thresholds: site-bond percolation phase diagram **6**

5. Critical exponents and universality **11**

6. Conclusions **14**

Acknowledgments **15**

Appendix **15**

A.1. Standard site percolation 15

A.2. Standard site percolation 16

References **17**

1. Introduction

The site-bond percolation problem is one of the central problems in statistical mechanics, and has attracted the attention othe researchers for several decades [1–18]. In this scheme, sites on a lattice are occupied with probability p_s and bonds or links between sites are opened with probability p_b. The occupation of sites and the opening of bonds are entirely independent and simultaneous processes. Then, it is possible to define *site–and–bond* ($S \cap B$) and *site–or–bond* ($S \cup B$) percolation: in $S \cap B$ ($S \cup B$), two points are said to be connected if a sequence of occupied sites *and* (*or*) bonds joins them. Thus, in $S \cap B$, a cluster is considered to be a set of occupied bonds and sites in which the bonds are joined by occupied sites, and the sites are joined by occupied bonds. In $S \cup B$, a bond or site contributes to cluster connectivity independently of the occupation of its endpoints[3].

The central idea of the site-bond percolation theory is based on finding the minimum concentration of elements (sites and bonds) for which a cluster extends from one side to the opposite one of the lattice, and a second order phase transition occurs in the system. In the case of $S \cap B$ site-bond percolation, the problem has many applications in different fields and has been studied in a wide variety of geometries [8–15]. On the other hand, the $S \cup B$ model has been treated in the literature for square [16], triangular [17] and simple cubic [18] lattices.

[3] $S \cap B$ and $S \cup B$ models will be explained in detail in section 2.

doi:10.1088/1742-5468/aa58f2

J. Stat. Mech. (2017) 023206

More general percolation problems can be formulated by including deposition of elements occupying more than one site (k-mers). In this sense, the pure site percolation of polyatomic species has been studied by using numerical simulations [19–22]. Vandewalle *et al* [19] studied the percolation and jamming phenomena for straight rigid rods of size k on two-dimensional (2D) square lattices for values of k between 2–10. The authors found that the percolation threshold decreases with increasing chain length k. A similar behavior was observed by Cornette *et al* [20] for sizes k ranging from 1 to 15. In addition, an exhaustive calculation of the critical exponents revealed that the problem belongs to the random percolation universality class regardless of the size of k used in the experiment.

Kondrat and Pękalski [21] extended the study of [19] to larger lattices (lattice size $L = 30$, 100, 300, 1000 and 2500) and longer objects ($1 \leqslant k \leqslant 2000$). The results obtained revealed that the percolation threshold is a nonmonotonic function of the size k: it decreases for small rod sizes, goes through a minimum around $k = 13$, and finally increases for large segments. This singular behavior was corroborated in a recent paper by Lebovka *et al* [22].

Budinski-Petković *et al* [23] investigated percolation and jamming thresholds for random sequential adsorption (RSA) of extended objects on triangular lattices. Numerical simulations were performed for lattices with linear size up to $L = 1000$, and objects of different sizes and shapes (linear segments; angled objects; triangles and hexagons). It was found that for elongated shapes the percolation threshold monotonically decreases, while for more compact shapes it monotonically increases with the object size. In the case of compact objects such as triangles and hexagons, a no-percolation regime was observed. The absence of percolation has also been reported in the studies of RSA of large rectangular particles [24], squares [25], and bent particles [26] on a square lattice.

On the other hand, the complete site-bond percolation model in the presence of multisite occupancy has received considerably less attention in the literature [27, 28]. In [27], a generalization of the standard site-bond percolation problem, in which pairs of nearest-neighbor sites (site dimers) and pairs of nearest-neighbor bonds (bond dimers) are independently occupied, was studied on a square lattice. The complete phase diagram of the system was obtained. The dimer problem was also addressed by Gao *et al* [28], who investigated the process of dissociative adsorption of dimers and studied the percolating properties of the dissociated monomers as a function of both the concentration of dimers and the dissociation probability. A phase diagram separating a percolating from a nonpercolating region was obtained.

In contrast to the statistic for the simple particles, the degeneracy of arrangements of dimers is strongly influenced by the structure of the lattice space. Then, it is of interest and of value to inquire how a specific lattice structure influences the main percolation properties of deposited dimers. In this context, the aim of the present work is to extend the study in [27] to triangular lattices. The problem is not only of theoretical interest. In numerous systems of practical importance, where the adsorbed particles are in thermodynamic equilibrium, the spatial distribution of the adsorbate might be characterized by using the site-bond percolation model [28]. A complete summary about adsorption on triangular lattices can be found in [29–32], and references therein.

This paper is organized as follows: the model and the simulation scheme are described in sections 2 and 3, respectively. The calculation of the percolation thresholds and the

J. Stat. Mech. (2017) 023206

resulting phase diagram in the $p_s - p_b$ space is reported in section 4. The analysis of results obtained by using finite size scaling theory is presented in section 5. The main purpose of this section is to test the universality of the problem by determining the numerical values of the critical exponents of the phase transition. Finally, conclusions drawn are given in section 6.

2. The model

The dimer site-bond percolation problem is defined on a two-dimensional triangular lattice. In our computer simulations, we use a rhombus-shaped system of $L \times L$ sites (L rows and L columns), with open boundary conditions (see figure 1).

Starting from an initially empty lattice, site dimers and bonds are independently and randomly deposited with concentrations p_s and p_b, respectively. The process is done in two stages. First, a pair of nearest-neighbor sites is randomly selected; if it is vacant, the site dimer is then deposited on those sites. Otherwise, the attempt is rejected. The procedure is iterated until N_s site dimers are deposited on the lattice ($p_s = 2N_s/L^2$). In a second stage, a given bond is randomly chosen; if it is vacant, the bond is then dropped onto the lattice. Otherwise, the attempt is rejected. The procedure is iterated until N_b bonds are deposited and the desired concentration ($p_b = N_b/3L^2$) is reached.

In the filling process, objects of finite size (site dimers) are randomly deposited (irreversibly adsorbed) on an initially empty substrate or lattice with the restriction that they must not overlap with previously added objects. The quantity of interest is the fraction of total site (bond) lattice, $p_s(t)$ [$p_b(t)$], covered at time t by the deposited objects. In the case of sites, and due to the blocking of the lattice by the already randomly adsorbed site dimers, the limiting or 'jamming coverage', $p_s^j = p_s(t \to \infty)$, is less than that corresponding to the close packing ($p_s^j < 1$) [33]. Consequently, p_s [p_b] ranges from 0 to p_s^j [1] for objects occupying more than one site, and the total area in the p_s-p_b phase diagram is p_s^j.

The $S \cap B$ model can be considered as a correlated bond percolation problem, or a pure site problem in which one replaces the bond by a site with two neighbors. On the other hand, the $S \cup B$ model can also be thought of as a bond problem, but not seem to be expressible as a pure site problem. Then, in order to calculate the percolation threshold, we can now think of a mapping $\mathbf{L} \to \mathbf{L}'$ from the original site-bond lattice $\mathbf{L}$ to an effective bond lattice $\mathbf{L}'$ where each bond and its endpoints sites of $\mathbf{L}$ transforms into a bond one of $\mathbf{L}'$. The rules for the mapping depend on the studied problem. Thus, for *site-or-bond* percolation (see figure 1(b)):

(i) each occupied bond of L transforms into an occupied bond one of L′;
(ii) each empty bond with one or two empty endpoint sites of L transforms into an empty bond in L′; and
(iii) each empty bond with its occupied endpoint sites of L transforms into an occupied bond of L′.

J. Stat. Mech. (2017) 023206

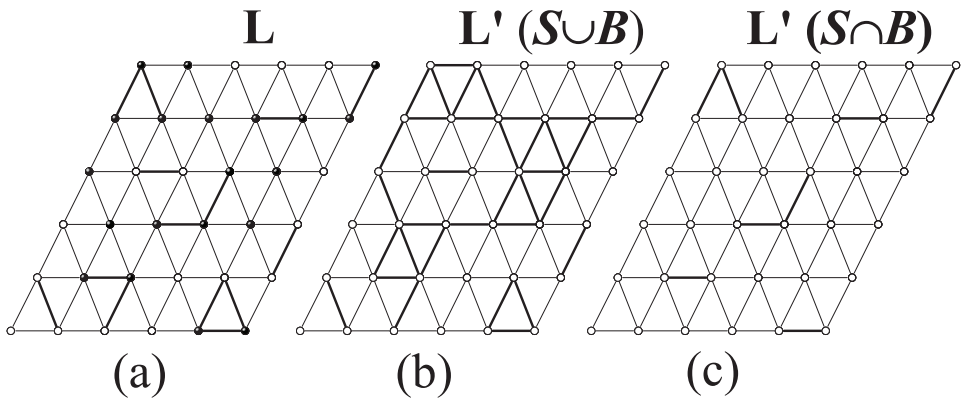

Figure 1. Rules for the mapping $\mathbf{L} \rightarrow \mathbf{L}'$ from an original site-bond lattice $\mathbf{L}$ (a) to an effective bond lattice $\mathbf{L}'$ for $S \cup B$ (b) and $S \cap B$ (c). Solid circles, open circles, thick lines and thin lines represent occupied sites, empty sites, occupied bonds and empty bonds, respectively.

On the other hand, for *site-and-bond* percolation (see figure 1(c)):

(i) each empty bond of L transforms into an empty one of L′;
(ii) each occupied bond with one or two empty endpoint sites of L transforms into an empty bond in L′; and
(iii) each occupied bond with its occupied endpoint sites of L transforms into an occupied bond of L′

Once the mapping is completed, each percolating/nonpercolating configuration in the effective lattice corresponds to a percolating/nonpercolating configuration in the original lattice. Then, the standard Hoshen and Kopelman algorithm [34] was applied for studying bond percolation on $\mathbf{L}'$.

3. Simulation scheme

It is well-known that it is quite a difficult matter to analytically determine the value of a percolation threshold for a given lattice [4]. For some special types of lattice, geometrical considerations enable their percolation thresholds to be derived exactly. For different conditions, i.e. for systems which do not present such a topological advantage, percolation thresholds have to be estimated numerically by means of computer simulations.

In the present case, each simulation run consists of the following three steps: (a) the construction of the triangular lattice for the desired fractions p_s and p_b of sites and bonds, respectively; (b) the mapping from the original site-bond lattice to the effective bond lattice; and (c) the cluster analysis by using the Hoshen and Kopelman algorithm [34] on the effective bond lattice. In the last step, the size of the largest cluster S_L is determined, as well as the existence of a percolating island. For this purpose, the probability $R_L^X(p_s, p_b)$ that a lattice composed of L^2 sites and $3L^2$ bonds percolates at the

J. Stat. Mech. (2017) 023206

concentration (p_s, p_b) can be defined. Here, the following definitions can be given according to the meaning of X [35]:

- $R_L^R(p_s, p_b)$: the probability of finding a rightward percolating cluster, along the x-direction,
- $R_L^D(p_s, p_b)$: the probability of finding a downward percolating cluster, along the y-direction.

Other useful definitions for the finite-size analysis are:

- $R_L^U(p_s, p_b)$: the probability of finding a cluster which percolates on any direction,
- $R_L^I(p_s, p_b)$: the probability of finding a cluster which percolates in the two (mutually perpendicular) directions,
- $R_L^A(p_s, p_b) = \frac{1}{2}[R_L^U(p_s, p_b) + R_L^I(p_s, p_b)]$.

A total of m_L independent runs of such three steps are carried out for obtaining the number m_L^X of them for which a percolating cluster of the desired criterion X is found. Then, $R_L^X(p_s, p_b) = m_L^X/m_L$ is defined. In the present study, a set of $m_L = 5 \times 10^5$ independent samples are numerically prepared for each model ($S \cup B$ and $S \cap B$), for each pair (p_s, p_b) and lattice size L ($L = 120$, 144, 180, 240, 480, 600). From the point of view of calculations, we set $p_s =$ constant and vary p_b.

In addition to the different probabilities $R_L^X(p_s, p_b)$, the percolation order parameter ($P = \langle S_L \rangle / M$) [36, 37] has been measured for each model, where $\langle ... \rangle$ means an average over simulation runs.

The quantities related with the order parameter, such as the susceptibility χ and the reduced fourth-order cumulant U_L introduced by Binder [38], can be calculated as

$$\chi = [\langle S_L^2 \rangle - \langle S_L \rangle^2]/3L^2, \tag{1}$$

and

$$U_L = 1 - \frac{\langle S_L^4 \rangle}{3\langle S_L^2 \rangle^2}. \tag{2}$$

4. Percolation thresholds: site-bond percolation phase diagram

As already explained, percolation is determined for 5×10^5 runs for each concentration (p_s, p_b), on each lattice size L, for each model ($S \cup B$ and $S \cap B$), and for each percolation criterion ($X = R$, D, I, U, A). The probabilities R_L^I, R_L^U and R_L^A are reported in figure 2 for two typical cases: (a) $S \cup B$ percolation and $p_s = 0.35$; and (b) $S \cap B$ percolation and $p_s = 0.70$. In both cases, p_b is varied during the simulation process.

From a simple inspection of figure 2, it is observed that R_L^X curves cross each other in a unique point R^{X^*}. The value of R^{X^*} depends on the criterion X used: $R^{A^*} \approx 0.5603$,

J. Stat. Mech. (2017) 023206

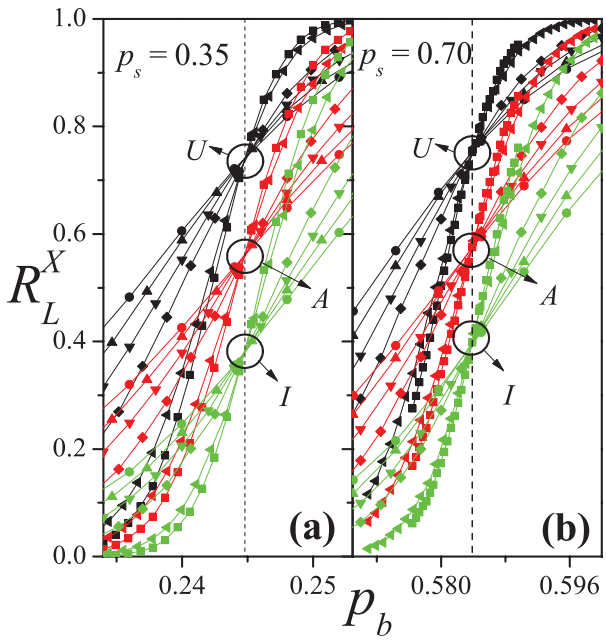

Figure 2. Fraction of percolating lattices R_L^X ($X = I$, U, A as indicated) as a function of the bond concentration p_b for two typical cases: (a) $S \cup B$ model and $p_s = 0.35$; and (b) $S \cap B$ model and $p_s = 0.70$. For each criterion, different lattice sizes were considered: $L = 120$, circles; 144, up triangles; 180, down triangles; 240, diamonds; 480, left triangles; and 600, squares. Horizontal dashed lines show the R^{X^*} universal points. Vertical dashed lines denote the percolation thresholds $p_{b,c}$ in the thermodynamic limit $L \to \infty$.

$R^{I^*} \approx 0.3803$ and $R^{U^*} \approx 0.7427$. In addition, the crossing points do not modify their numerical value for the different studied cases, as a first indication that the problem belongs to the same universality class no matter the model ($S \cup B$ or $S \cap B$) and the value of p_s used in the experiment.

In the case of dimer site-bond percolation on square lattices with periodic boundary conditions, the values of R^{X^*} reported in [27] were: $R^{A^*} \approx 0.453$, $R^{I^*} \approx 0.259$ and $R^{U^*} \approx 0.622$. The differences can be attributed to the differences in shape and boundary conditions between the system studied here and the system investigated in [27].

It is also interesting to compare the values of R^{X^*} obtained in figure 2 with the ones corresponding to standard site percolation and standard bond percolation on a rhombus-shaped lattice with open boundary conditions: $R^{A^*} \approx 0.501$; $R^{I^*} \approx 0.311$ and $R^{U^*} \approx 0.687$ (pure site percolation); and $R^{A^*} \approx 0.508$, $R^{I^*} \approx 0.319$ and $R^{U^*} \approx 0.693$ (pure bond percolation). Further details on the calculations are provided in the appendix. These differences between the values of R^{X^*} for the mixed site-bond percolation problem and the pure site (and bond) percolation have already been observed for square lattices [20, 27].

In the vicinity of the critical point, cumulants show a strong dependence on the system size. However, at the critical point the cumulants adopt a constant value, irrespective of system sizes in the scaling limit. Thus, the measure of the intersection point of the cumulants, U^*, is of importance to understand the critical behavior of the system

J. Stat. Mech. (2017) 023206

[38]. In this line, the intersection point of the cumulants was obtained for different concentrations (p_s, p_b). In all cases, the value of U^* remains constant around $U^* \approx 0.544$ no matter the model ($S \cup B$ or $S \cap B$) used in the experiment.

In order to compare with the value of U^* obtained for mixed site-bond models, the intersection point of the cumulants was calculated for standard site percolation and standard bond percolation on a rhombus-shaped lattice with open boundary conditions. As shown in appendix, $U^* \approx 0.538$ (site percolation) and $U^* \approx 0.532$ (bond percolation).

As occurred with the crossing point of the percolation probabilities, the behavior of U^* changes for the site-bond percolation problem, with respect to the pure site percolation problem and the pure bond percolation problem. The values of U^* obtained in the appendix also differ with respect to the value $U^* \approx 0.555$ reported by Machado *et al* [39] for random bond percolation on a square lattice with a square boundary. This finding indicates that, as expected, the measure of U^* depends on the shape of the lattice.

In order to express $R_L^X(p_s, p_b)$ as a function of continuous values of p_b, it is convenient to fit $R_L^X(p_s, p_b)$ with some approximating function through the least-squares method. The fitting curve is the *error function* because $\mathrm{d}R_L^X/\mathrm{d}p_b$ is expected to behave like the Gaussian distribution[4]

$$\frac{\mathrm{d}R_L^X}{\mathrm{d}p_b} = \frac{1}{\sqrt{2\pi}\,\Delta_L^X} \exp\left\{-\frac{1}{2}\left[\frac{p_b - p_{b,c}^X(L)}{\Delta_L^X}\right]^2\right\}, \tag{3}$$

where $p_{b,c}^X(L)$ is the concentration at which the slope of $R_L^X(p_s, p_b)$ is the largest and Δ_L^X is the standard deviation from $p_{b,c}^X(L)$.

The percolation threshold $p_{b,c}$ can be obtained from the extrapolation of the positions $p_{b,c}^X(L)$ of the maxima of the slopes of $R_L^X(p_s, p_b)$. Thus, for each criterion (I, U and A), for each percolation model ($S \cup B$ and $S \cap B$) and for each value of p_s, one expects that [4]

$$p_{b,c}^X(L) = p_{b,c} + A^X L^{-1/\nu}, \tag{4}$$

where A^X is a nonuniversal constant and ν is the critical exponent of the correlation length which will be taken as 4/3 for the present analysis, since, as it will be shown in section 5, our model belongs to the same universality class as random percolation [4].

Figure 3 shows the plots towards the thermodynamic limit of $p_{b,c}^X(L)$ according to equation (4) for the data in figure 2. From extrapolations it is possible to obtain the percolation thresholds for the criteria I, A and U. Combining the three estimates for each case, the final values of $p_{b,c}$ can be obtained. Additionally, the maximum of the differences between $|p_{b,c}^U - p_{b,c}^A|$ and $|p_{b,c}^I - p_{b,c}^A|$ gives the error bar for each determination of $p_{b,c}$. In this case, the values obtained were: $p_{b,c} = 0.2448(1)$ (a), and $p_{b,c} = 0.5839(2)$ (b).

The procedure in figure 3 was repeated for different values of p_s. The results, which are shown in figure 4 and collected in tables 1 and 2, (i) represent the complete phase diagram of the system in the (p_s, p_b) space, and (ii) are reported for the first time in the

[4] Even though the behavior of $\mathrm{d}R_L^X/\mathrm{d}p_b$ is known not to be a Gaussian in all range of p_b, this quantity is approximately Gaussian near the peak, and equation (3) is a good approximation for the purpose of locating its maximum [40].

J. Stat. Mech. (2017) 023206

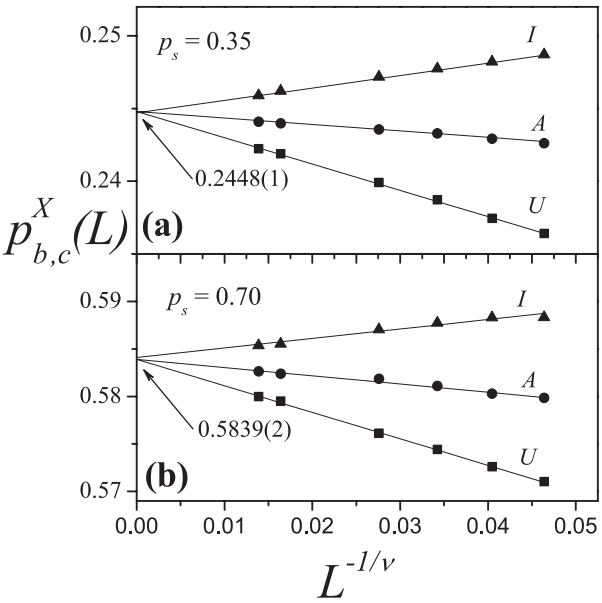

Figure 3. Extrapolation of $p^X_{b,c}(L)$, towards the thermodynamic limit according to the theoretical prediction given by equation (4). Triangles, circles and squares denote the values of $p^X_{b,c}(L)$, obtained by using the criteria I, A and U, respectively. (a) $S \cup B$ model and $p_s = 0.35$. (b) $S \cap B$ model and $p_s = 0.70$.

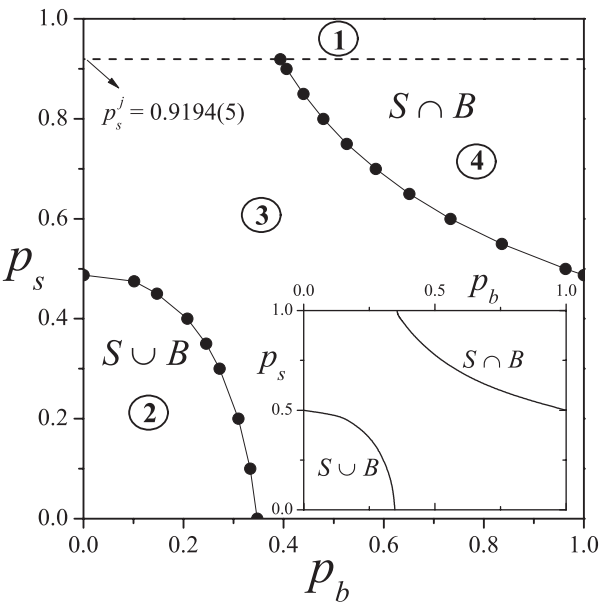

Figure 4. Phase diagram of dimer site-bond percolation on triangular lattices. Inset: phase diagram for standard site-bond percolation on triangular lattices, as reported in [17].

J. Stat. Mech. (2017) 023206

Table 1. Numerical values of (p_s, p_b) for the critical line corresponding to the $S \cup B$ percolation model. Error estimates concerning the last digit are indicated between brackets.

p_s	p_b
0	0.347 296 355...
0.10	0.3332(2)
0.20	0.3094(1)
0.30	0.2718(1)
0.35	0.2448(1)
0.40	0.2072(4)
0.45	0.1468(3)
0.475	0.1011(5)
0.4872(8)	0

Table 2. Numerical values of (p_s, p_b) for the critical line corresponding to the $S \cap B$ percolation model. Error estimates concerning the last digit are indicated between brackets.

p_s	p_b
0.4872(8)	1
0.50	0.9634(4)
0.55	0.8359(5)
0.60	0.7337(3)
0.65	0.6515(1)
0.70	0.5839(2)
0.75	0.5259(3)
0.80	0.4792(3)
0.85	0.4394(5)
0.90	0.4055(4)
0.9194(5)	0.3931...

present study. To summarize the results in the figure, four regions were indicated in the phase diagram. Region 1: forbidden region ($p_s > p_s^j$); region 2: nonpercolating region for $S \cup B$ and $S \cap B$ models; region 3, percolating region for $S \cup B$ model, and nonpercolating region for $S \cap B$ model; and region 4, percolating region for $S \cup B$ and $S \cap B$ models.

In the case of $S \cup B$ model, the critical curve separating the percolating and nonpercolating regions varies between the point $[p_s = 0.4872(8), p_b = 0.0]$ at left, and the point $[p_s = 0.0, p_b = 0.347\,296\,355...]$ at right. $p_b = 0.347\,296\,355...$ [41] $[p_s = 0.4872(8)$ [43] represents the percolation threshold for the standard bond (site dimer) percolation on a triangular lattice. The value 0.347 296 355... has also been recently reported for the problem of fully dimer-covered lattices [44]. In [44], the authors showed that the shifted covering of the square lattice is topologically identical to the triangular lattice with its percolation threshold of 0.347 296 355.... An extensive list of percolation thresholds for $d \in [2, 13]$ (d is the dimension of the space) can be found on the Wikipedia webpage: https://en.wikipedia.org/wiki/Percolation_threshold.

On the other hand, the line of threshold values corresponding to the $S \cap B$ percolation model varies between the point $[p_s^j = 0.9194(5), p_b = 0.3931...]$ at left, and the point $[p_s = 0.4872(8), p_b = 1.0]$ at right. $p_s^j = 0.9194(5)$ [23, 42] is the jamming coverage

J. Stat. Mech. (2017) 023206

corresponding to site dimers on triangular lattices, and the value $p_b = 0.3931...$ was obtained by extrapolation.

As mentioned above, (1) standard site dimer percolation is recovered as $p_b = 0.0$ and $p_b = 1.0$; and (2) standard bond percolation is recovered as $p_s = 0.0$.

The areas of the percolating and nonpercolating regions vary with respect to the corresponding ones for standard site-bond percolation [17] (see inset in figure 4). Thus, the percolating (nonpercolating) area for $S \cup B$ model changes from 0.8611 (0.1389) for standard site-bond percolation to 0.7876 (0.1318) for dimer site-bond percolation. On the other hand, the percolating (nonpercolating) area for $S \cap B$ model changes from 0.2135 (0.7865) for standard site-bond percolation to 0.1652 (0.7542) for dimer site-bond percolation.

5. Critical exponents and universality

As shown in the previous section and appendix, the crossing points R^{X^*} and U^* vary for the site-bond percolation problem, with respect to the pure site percolation problem and the pure bond percolation problem. This behavior was also observed for square lattices [27]. In the case of thermal transitions, the link between universality class and the behavior of the intersection point of the cumulants has been discussed in [45, 46]. In fact, as pointed out by Selke and Shchur [45] and Selke [46], the measure of the cumulant intersection may depend on various details of the model, which do not affect the universality class.

In [27], the authors showed that, even though changes were observed in the values of R^{X^*}, the dimer site-bond percolation problem on square lattices belongs to the standard percolation universality class. In order to confirm or discard this hypothesis for triangular lattices, the critical exponents ν, β and γ will be calculated. Critical exponents are of importance because they describe the universality class of a system and allow for the understanding of the related phenomena.

The standard theory of finite-size scaling [4] allows for various efficient routes to estimate the critical exponent ν from simulation data. One of these methods is from the maximum of the function in equation (3),

$$\left(\frac{\mathrm{d}R_L^X}{\mathrm{d}p_b}\right)_{\max} \propto L^{1/\nu}. \tag{5}$$

In figure 5(a), $\log\left[(\mathrm{d}R_L^A/\mathrm{d}p_b)_{\max}\right]$ has been plotted as a function of $\log[L]$ (note the log–log functional dependence) for the same cases in figures 2 and 3. According to equation (5) the slope of each line corresponds to $1/\nu$. As it can be observed, the slopes of the curves remain constant. Thus, $\nu = 1.33(4)$ for $p_s = 0.35$ ($S \cup B$), and $\nu = 1.35(5)$ for $p_s = 0.70$ ($S \cap B$).

Another alternative way for evaluating ν is from the divergence of the root mean square deviation of the threshold observed from their average values, Δ_L^X,

$$\Delta_L^X \propto L^{-1/\nu}. \tag{6}$$

J. Stat. Mech. (2017) 023206

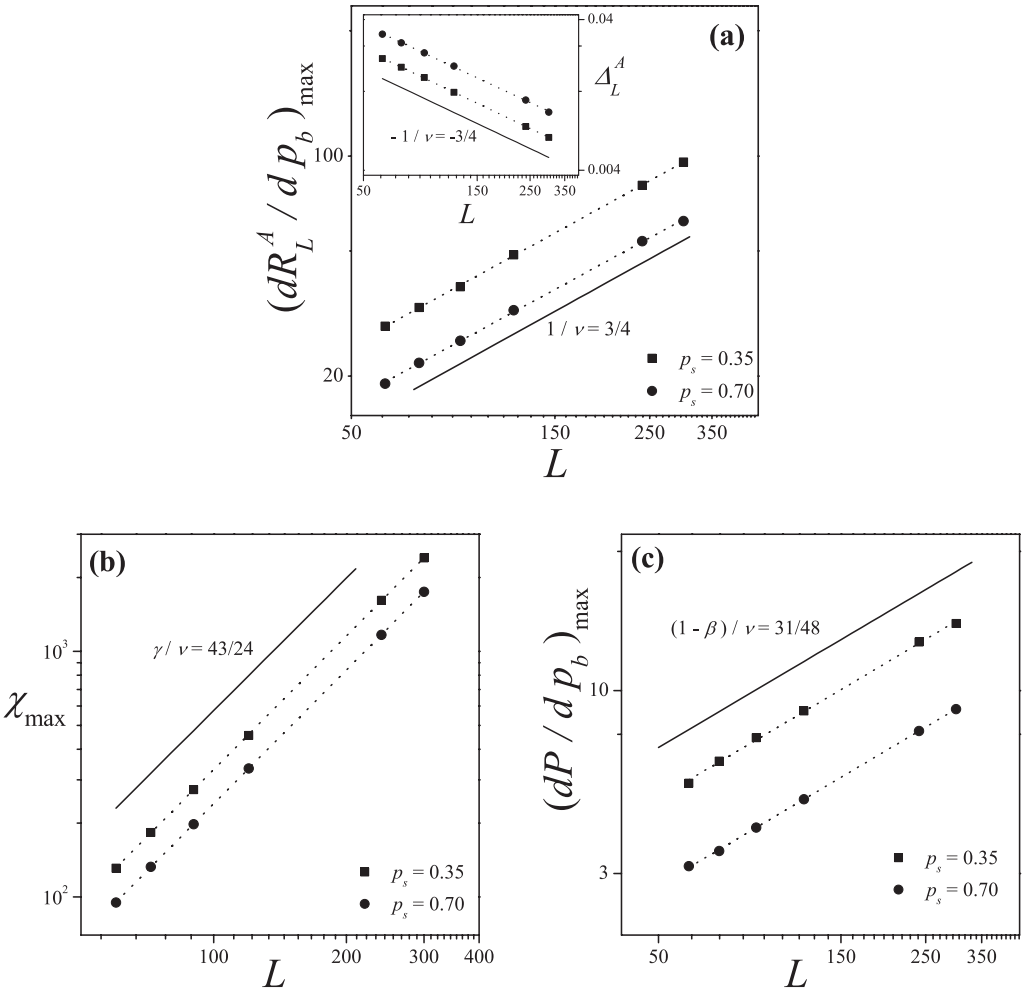

Figure 5. (a) Log–log plot of $(\mathrm{d}R_L^A/\mathrm{d}p_b)_{\max}$ as a function of L for $S\cup B$ ($p_s = 0.35$) and $S\cap B$ ($p_s = 0.70$). According to equation (5) the slope of the curve corresponds to $1/\nu$. Inset: $\log \Delta_L^A$ as a function of L for the same case in the main figure. According to equation (6), the slope of the curve corresponds to $-1/\nu$. (b) Log–log plot of $\chi_{\max}$ as a function of L for the cases in part (a). The slope of each line corresponds to $\gamma/\nu = 43/24$. (c) Log–log plot of $(\mathrm{d}P/\mathrm{d}p_b)_{\max}$ as a function of L for the cases in parts (a) and (b). According to equation (8), the slope of each curve corresponds to $(1-\beta)/\nu = 31/48$.

As an example of the validity of the last equation, the insets in figure 5(a) shows Δ_L^A as a function of L (note the log–log scale) for the same cases in the main figure. According to equation (6), the slope of the line corresponds to $-1/\nu$. In this case, $\nu = 1.33(1)$ ($p_s = 0.35$, $S\cup B$) and $\nu = 1.35(3)$ ($p_s = 0.70$, $S\cap B$).

The study in figure 5(a) was repeated for different values of p_s and the I, U and A criteria. In all cases, the results obtained for ν coincide within numerical errors with the exact value of the critical exponent of the ordinary 2D percolation, namely, $\nu = 4/3$ [4].

Once we know ν, the exponent γ can be determined by scaling the maximum value of the susceptibility equation (1). According to the finite-size scaling theory [4], the

J. Stat. Mech. (2017) 023206

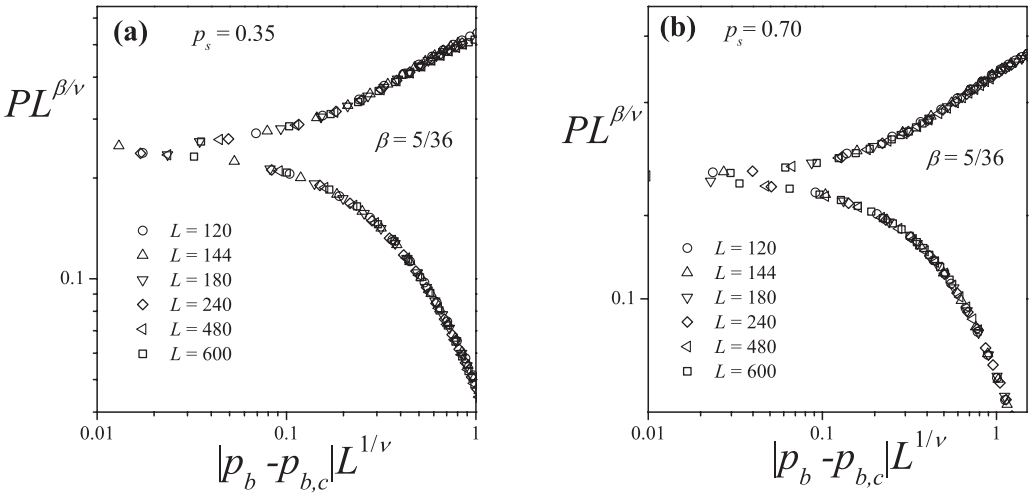

Figure 6. (a) Data collapsing of the percolation order parameter, $PL^{\beta/\nu}$ versus $|p_b - p_{b,c}|L^{1/\nu}$, for $S \cup B$ ($p_s = 0.35$) (a) and $S \cap B$ ($p_s = 0.70$) (b). The plots were made using the exact percolation exponents $\nu = 4/3$ and $\beta = 5/36$.

behavior of χ at criticality is $\chi = L^{\gamma/\nu}\overline{\chi}(u)$, where $u = (p_b - p_{b,c})L^{1/\nu}$ and $\overline{\chi}$ is the corresponding scaling function. At the point where χ is maximal, $u =$ const. and $\chi_{\max} \propto L^{\gamma/\nu}$. Our data for $\chi_{\max}$ are shown in figure 5(b). The values obtained are $\gamma = 2.41(4)$ for $S \cup B$ ($p_s = 0.35$), and $\gamma = 2.41(3)$ for $S \cap B$ ($p_s = 0.70$). Simulation data are consistent with the exact value of the critical exponent of the ordinary percolation, $\gamma = 43/18$.

On the other hand, the standard way to extract the exponent ratio β is to study the scaling behavior of P at criticality [4],

$$P = L^{-\beta/\nu}\overline{P}(u'), \tag{7}$$

where $u' = |p_b - p_{b,c}|L^{1/\nu}$ and $\overline{P}$ is the scaling function. At the point where $\mathrm{d}P/\mathrm{d}p_b$ is maximal, $u =$ const. and

$$\left(\frac{\mathrm{d}P}{\mathrm{d}p_b}\right)_{\max} = L^{(-\beta/\nu+1/\nu)}\overline{P}(u') \propto L^{(1-\beta)/\nu}. \tag{8}$$

The scaling of $(\mathrm{d}P/\mathrm{d}p_b)_{\max}$ is shown in figure 5(c) for the cases in parts (a) and (b). From the slopes of the curves, the following values of β were obtained: $\beta = 0.135(4)$ for $S \cup B$ ($p_s = 0.35$) and $\beta = 0.136(3)$ for $S \cap B$ ($p_s = 0.70$). These results agree very well with the exact value of β for ordinary percolation, $\beta = 5/36$.

The values calculated for ν (figure 5(a)), γ (figure 5(b)) and β (figure 5(c)) clearly indicate that this problem belongs to the same universality class that the random percolation regardless the model ($S \cup B$ or $S \cap B$) and the value of p_s considered.

The scaling behavior can be further tested by plotting U_L versus $(p_b - p_{b,c})L^{\frac{1}{\nu}}$, $PL^{\beta/\nu}$ versus $|p_b - p_{b,c}|L^{1/\nu}$ and $\chi L^{-\gamma/\nu}$ versus $(p_b - p_{b,c})L^{1/\nu}$ and looking for data collapsing [4]. Using the values of $p_{b,c}$ calculated above and the exact values of the critical exponents of the ordinary percolation $\nu = 4/3$, $\beta = 5/36$ and $\gamma = 43/18$, we obtain an excellent

J. Stat. Mech. (2017) 023206

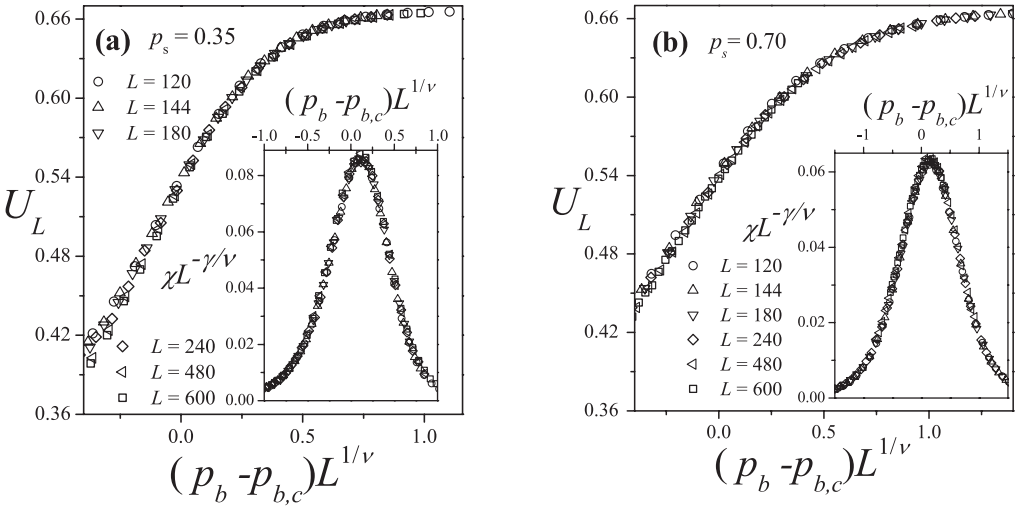

Figure 7. Data collapsing of the cumulant, U_L versus $(p_b - p_{b,c})L^{1/\nu}$, and of the susceptibility, $\chi L^{-\gamma/\nu}$ versus $(p_b - p_{b,c})L^{1/\nu}$ (inset), for $S \cup B$ ($p_s = 0.35$) (a) and $S \cap B$ ($p_s = 0.70$) (b). The plots were made using the exact percolation exponents $\nu = 4/3$ and $\gamma = 43/18$.

scaling collapse as it is shown in figures 6 and 7 for the cases discussed in previous figures. This leads to independent controls and consistency checks of the values of all the critical exponents.

6. Conclusions

In the present work, the site-bond percolation problem for dimers on triangular lattices has been addressed. Two distinct schemes, site-and-bond ($S \cap B$) and site-or-bond ($S \cup B$), have been considered. In $S \cap B$, a cluster is considered to be a set of occupied bonds and sites in which the bonds are joined by occupied sites, and the sites are joined by occupied bonds. In $S \cup B$, a bond or site contributes to cluster connectivity independently of the occupation of its endpoints.

For $S \cap B$ model, the jamming coverage (the percolation threshold) corresponding to dimers on triangular lattices determines the left (right) limit of the critical curve. In the case of $S \cup B$, the critical line is limited by the percolation threshold of dimers (at left) and the percolation threshold of bonds (at right). The complete phase diagram ($S \cup B$ and $S \cap B$ critical lines separating the percolating and nonpercolating regions) is presented for the first time in the literature.

The values of the crossing point of the percolation probabilities R^{X^*} and the intersection point of the cumulants U^* were measured for mixed site-bond percolation ($S \cup B$ or $S \cap B$ models), standard site percolation and standard bond percolation on a rhombus-shaped $L \times L$ lattice with open boundary conditions. Finally, the accurate determination of the critical exponents revealed that, in all cases, the problem belongs to the same universality class as 2D random percolation model.

J. Stat. Mech. (2017) 023206

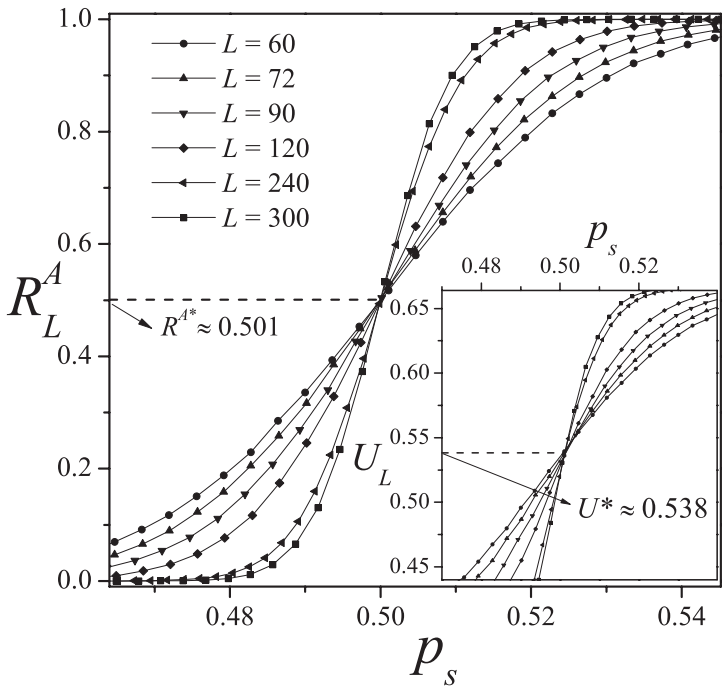

Figure A1. Fraction of percolating lattices R_L^A and cumulants U_L (inset) as a function of p_s for standard site percolation on a rhombus-shaped $L \times L$ lattice with open boundary conditions. Different lattice sizes were considered: $L = 60$, circles; $L = 72$, up triangles; $L = 90$, down triangles; $L = 120$, diamonds; $L = 240$, left triangles; and $L = 300$, squares.

Acknowledgments

This work was supported in part by CONICET (Argentina) under project number PIP 112-201101-00615; Universidad Nacional de San Luis (Argentina) under project 322000; and the National Agency of Scientific and Technological Promotion (Argentina) under project PICT-2013-1678. The numerical work were done using the BACO3 parallel cluster (composed by 50 PCs each with an Intel i7-3370/2600 processor) located at Instituto de Física Aplicada, Universidad Nacional de San Luis - CONICET, San Luis, Argentina.

Appendix

In this section, the crossing points of the percolation probabilities (R^{A^*}, R^{I^*} and R^{U^*}) and the intersection point of the cumulants (U^*) will be obtained for (1) standard site percolation and (2) standard bond percolation on triangular lattices. In both cases, the elements (sites/bonds) will be deposited on a rhombus-shaped $L \times L$ lattice with open boundary conditions as discussed in section 2.

A.1. Standard site percolation

Starting from an initially empty lattice, a site is randomly selected; if it is vacant, the site is occupied. Otherwise, the attempt is rejected. The procedure is iterated until N_s

J. Stat. Mech. (2017) 023206

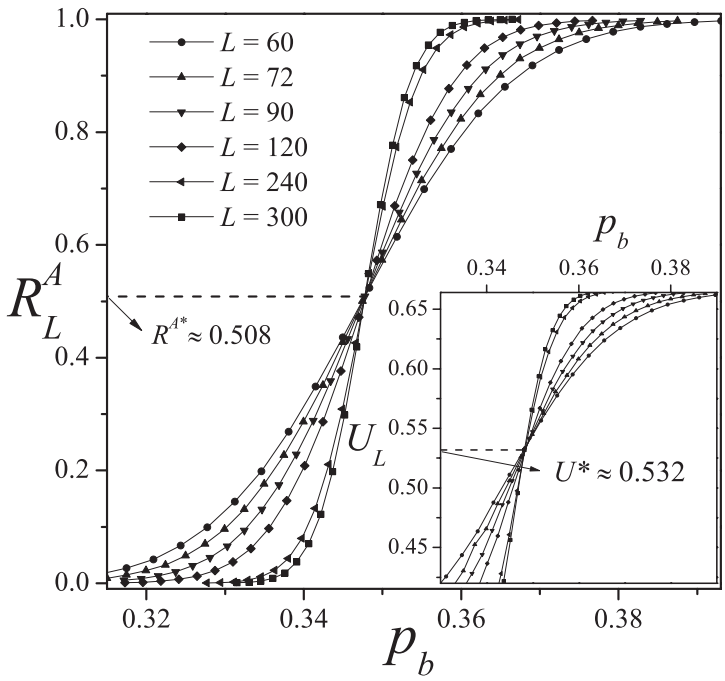

Figure A2. Fraction of percolating lattices R_L^A and cumulants U_L (inset) as a function of p_b for standard bond percolation on a rhombus-shaped $L \times L$ lattice with open boundary conditions. Different lattice sizes were considered: $L = 60$, circles; $L = 72$, up triangles; $L = 90$, down triangles; $L = 120$, diamonds; $L = 240$, left triangles; and $L = 300$, squares.

sites are occupied and $p_s = N_s/L^2$. Then, the Hoshen and Kopelman algorithm is applied [34]. In the last step, the size of the largest cluster S_L is determined, as well as the existence of a percolating island of occupied sites and the calculation of the probabilities $R_L^A(p_s)$, $R_L^I(p_s)$ and $R_L^U(p_s)$.

The procedure above is repeated for different both values of p_s and lattice sizes. A set of 10^5 independent samples are numerically prepared for each value of p_s and L ($L = 60$, 72, 90, 120, 240, 300).

The probabilities R_L^A and the cumulants U_L (inset) are reported in figure A1 for different lattice sizes (curves corresponding to R_L^I and R_L^U are not shown for the sake of clarity). The values obtained for the crossing points are: $R^{A^*} \approx 0.501$, $R^{I^*} \approx 0.311$, $R^{U^*} \approx 0.687$ and $U^* \approx 0.538$. In addition, these critical points are located at a well-defined value in the p_s-axes determining the percolation threshold of the system $p_{s,c}$. In this case, $p_{s,c} \approx 0.50$, which is consistent with the exact critical threshold for the standard site percolation on triangular lattices $p_{s,c} = 1/2$ [41].

A.2. Standard site percolation

Starting from an initially empty lattice, a bond is randomly selected; if it is vacant, the bond is occupied. Otherwise, the attempt is rejected. The procedure is iterated until N_b bonds are occupied and $p_b = N_b/3L^2$. As in the previous case, the Hoshen and Kopelman

J. Stat. Mech. (2017) 023206

algorithm is used [34] (applied this time to the different clusters of occupied bonds) and the quantities of interest are measured over a set of 10^5 independent runs for each value of p_s and L ($L = 60$, 72, 90, 120, 240, 300).

Figure A2 shows the results obtained for the percolation probabilities R_L^A and the cumulants (as in figure A1, the curves corresponding to R_L^I and R_L^U are not shown). In this case, $R^{A^*} \approx 0.508$, $R^{I^*} \approx 0.319$, $R^{U^*} \approx 0.693$ and $U^* \approx 0.532$. On the other hand, the value of the percolation threshold obtained from simulation $p_{b,c} \approx 0.347$ coincides, within the statistical errors, with the well-known threshold for the standard bond percolation on triangular lattices $p_{b,c} = 0.347\,296\,355...$ [41].

References

[1] Broadbent S R and Hammersley J M 1957 *Proc. Camb. Phil. Soc.* **53** 629
Broadbent S R and Hammersley J M 1957 *Proc. Camb. Phil. Soc.* **53** 642
[2] Kesten H 1982 *Percolation Theory for Mathematicians* (Boston, MA: Birkhäuser)
[3] Zallen R 1983 *The Physics of Amorphous Solids* (New York: Wiley)
[4] Stauffer D and Aharony A 1985 *Introduction to Percolation Theory* 2nd edn (London: Taylor and Francis)
[5] Sahimi M 1994 *Applications of percolation theory* (London: Taylor and Francis)
Sahimi M 1995 *Flow and transport in Porous Media and Fractured Rock* (Weinhein: VCH)
[6] Grimmett G 1999 *Percolation* (Berlin: Springer)
[7] Bollobás B and Riordan O 2006 *Percolation* (Cambridge: Cambridge University Press)
[8] Coniglio A, Stanley H E and Klein W 1979 *Phys. Rev. Lett.* **42** 518
[9] Frisch H L and Hammersley J M 1963 *J. Soc. Ind. Appl. Math.* **11** 894
[10] Agrawal P, Render S, Reynolds P J and Stanley H E 1979 *J. Phys. A: Math. Gen.* **12** 2073
[11] Nakanishi H and Reynolds P J 1979 *Phys. Lett.* **71** A 252
[12] Yanuka M and Englman R 1990 *J. Phys. A: Math. Gen.* **23** L339
[13] Tarasevich Y Y and van der Marck S C 1999 *Int. J. Mod. Phys.* C **10** 1193
[14] Ziff R M and Gu H 2009 *Phys. Rev.* E **79** 020102
[15] Nduwayo L, Lindebaum R and Chetty N 2009 *Comput. Phys. Commun.* **180** 503
[16] Tsallis C and de Magalhães A C N 1996 *Phys. Rep.* **268** 305
[17] González M I, Centres P M, Lebrecht W, Ramirez-Pastor A J and Nieto F 2013 *Physica* A **392** 6330
[18] González M I, Centres P M, Lebrecht W and Ramirez-Pastor A J 2016 *J. Stat. Mech.* 093210
[19] Vandewalle N, Galam S and Kramer M 2000 *Eur. Phys. J.* B **14** 407
[20] Cornette V, Ramirez-Pastor A J and Nieto F 2003 *Eur. Phys. J.* B **36** 391
[21] Kondrat G and Pękalski A 2001 *Phys. Rev.* E **63** 051108
[22] Lebovka N I, Karmazina N N, Tarasevich Y Y and Laptev V V 2011 *Phys. Rev.* E **84** 061603
[23] Budinski-Petković Lj, Loncarević I, Petković M, Jaksić Z M and Vrhovac S B 2012 *Phys. Rev.* E **85** 061117
[24] Porto M and Roman H E 2000 *Phys. Rev.* E **62** 100
[25] Nakamura M 1987 *Phys. Rev.* A **36** 2384
[26] Kondrat G 2008 *Phys. Rev.* E **78** 011101
[27] Dolz M, Nieto F and Ramirez-Pastor A J 2005 *Eur. Phys. J.* B **43** 363
[28] Gao Z and Yang Z R 1998 *Physica* A **255** 242
[29] Phares A J, Grumbine D W Jr and Wunderlich F J 2006 *Langmuir* **22** 7646
[30] Phares A J, Grumbine D W Jr and Wunderlich F J 2007 *Langmuir* **23** 1928
[31] Phares A J, Grumbine D W Jr and Wunderlich F J 2008 *Langmuir* **24** 124
[32] Phares A J, Grumbine D W Jr and Wunderlich F J 2009 *Langmuir* **25** 944
[33] Evans J W 1993 *Rev. Mod. Phys.* **65** 1281
[34] Hoshen J and Kopelman R 1976 *Phys. Rev.* B **14** 3438
Hoshen J, Kopelman R and Monberg E M 1978 *J. Stat. Phys.* **19** 219
[35] Yonezawa F, Sakamoto S and Hori M 1989 *Phys. Rev.* B **40** 636
Yonezawa F, Sakamoto S and Hori M 1989 *Phys. Rev.* B **40** 650
[36] Biswas S, Kundu A and Chandra A K 2011 *Phys. Rev.* E **83** 021109
[37] Chandra A K 2012 *Phys. Rev.* E **85** 021149
[38] Binder K 1997 *Rep. Prog. Phys.* **60** 488
[39] Machado E, Buendía G M, Rikvold P A and Ziff R M 2005 *Phys. Rev.* E **71** 016120

[40] Newman M E J and Ziff R M 2001 *Phys. Rev.* E **64** 016706
[41] Sykes M F and Essam J W 1964 *J. Math. Phys.* **5** 1117
[42] Budinski-Petković Lj, Lončarević I, Jakšić Z M and Vrhovac S B 2016 *J. Stat. Mech.* 053101
[43] Cornette V, Ramirez-Pastor A J and Nieto F 2003 *Physica* A **327** 71
[44] Haji-Akbari A, Haji-Akbari N and Ziff R M 2015 *Phys. Rev.* E **92** 032134
[45] Selke W and Shchur L N 2005 *J. Phys. A: Math. Theor.* **38** L739
[46] Selke W 2007 *J. Stat. Mech.* P04008

J. Stat. Mech. (2017) 023206